Multi-fluid Euler-Euler model of the blood flow within the blood vessel with rigid walls

Maria Gracka[*][†]

Key words: CFD, Euler-Euler model, multi-fluid, blood flow, aorta

Abstract

The cardiovascular diseases and disorders such as atherosclerosis, strokes and heart attacks are the leading causes of death in the world mainly in the developed and industrialized societies. Understanding of basic mechanisms and phenomena occurring in the cardiovascular system could be useful in early detection of the development of lesions in blood vessels. In the presented work numerical analysis of blood flow within aorta has been made. Analysis included two models: single- and multi-phase approaches. In first blood was treated as a homogenous, non-Newtonian fluid with averaged rheological properties of viscosity and density. Second model uses an Eulerian multiphase approach in model of blood flow which assumes blood as a mixture of three phases (plasma, erythrocytes and leukocytes). To develop numerical model of blood flow within the human blood vessel the commercial software ANSYS Fluent (ANSYS Inc., USA) has been used. In the project the geometry of 8-year old patient with moderate thoracic aortic coarctation (approximately 65% area reduction) has been used. The geometry was created from data generated during Gadolinium-enhanced MR angiography (MRA). Model of the geometry includes ascending aorta, arch, descending aorta und upper branches such as innominate artery, left common artery, left subclavian artery. To reproduce periodic cardiac cycle as an inlet boundary condition velocity profile was used. Velocity profile was calculated from the conversion of the volumetric flow that was measured by a phase-contrast (PC) MRI sequence with through-plane velocity encoding. As the outlet boundary conditions for all branches and descending aorta the outflow condition was used. Volumetric share of blood flow through various outflows of the aortic model was measured via PC-MRI. Results of numerical simulation are presented for two characteristic points (during systole and diastole) of the cardiac cycle.

29

1. Introduction

The cardiovascular diseases and disorders such as atherosclerosis, strokes and heart attacks are the leading causes of death in the world mainly in the developed and industrialized societies. Understanding of basic mechanisms and phenomena occurring in the cardiovascular system could be useful in early detection of the development of lesions in blood vessels, where pharmacologic treatment can be used instead of expensive and complicated surgical procedures [12]. Computer models offer many advantages over experimental work therefore, in recent years Computational Fluid Dynamics (CFD) methods [14], widely used in various engineering applications, have become a tool and proved its applicability in the biomedical flows modeling. Computer models can be used to perform virtual experiments that can give answers related to flow conditions in human body. Increasingly numerical modeling is used in the design of medical devices such as stents, artificial hearts and heart valves. The accurate velocity and pressure fields obtained in simulations could help in early medical diagnosis for instance to indicate on zones vulnerable to cardiac diseases.

1.1 The scope of the work

The scope of the present work shows an Eulerian multiphase approach in model of blood flow in human blood vessel (artery) section. Proposed numerical model assumes blood flow in rigid vessels and blood properties as a non-homogeneous fluid which consists of blood plasma, red blood cells (erythrocytes) and white blood cells (leukocytes). Multi-fluid Euler-Euler technique [8] allows to model the flow behavior for each of blood components and treat each phase as a separate interpenetrating continua with defined density, volume fraction and other physical properties [3].

1.2 ANSYS Fluent

To develop numerical model of blood flow within the human blood vessel the ANSYS Fluent (ANSYS Inc., USA), commercial CFD software has been used. The software allows modeling of all phenomena associated with the flows (combustion, turbulence, multiphase flows, chemical reactions, heat transfer, radiation and as well as flow condition in human body) and preparing geometry and mesh corresponding to the simulated phenomenon.

The numerical model of human artery and multi-fluid blood flow was prepared using ANSYS Fluent v.17, while flow equations of pulsatory boundary conditions were implemented by using User Defined Function (UDF). This approach covers the influence of the human arterial system and allows to reproduce periodical cardiac cycles that determinate the pulsating (transient) blood flow conditions.

2. Geometrical model

2.1 Geometry

In presented work the geometry of 8-year old patient with moderate thoracic aortic coarctation (approximately 65% area reduction) has been used. The geometry was created from data generated during Gadolinium-enhanced MR angiography (MRA) using 1.5 GE

Sigma scanner [17]. Figure 1 shows model of the aorta that includes ascending aorta (AAO), arch, descending aorta (DAO) und upper branches such as innominate artery (IA), left common artery (LCCA), left subclavian artery(LSA).
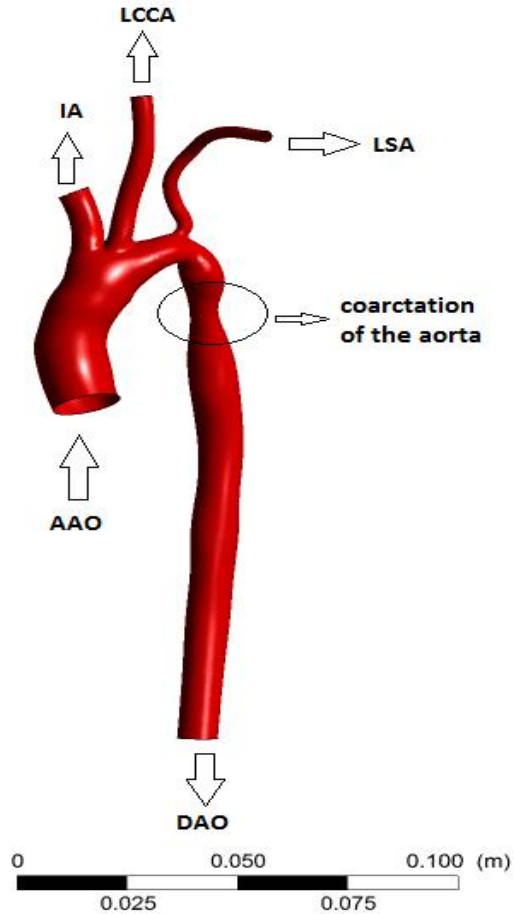

Figure 1: The geometry of the aorta with selected inlet and outlets used in CFD model

2.2 Mesh

In the modeling of phenomena characterized by a high irregularity significant impact on the accuracy, computation time and convergence of the solution has a number of numerical mesh divisions of the considered geometry. Mesh generated in the project is shown in Fig. 2 and Fig. 3 consists about 750 000 of hybrids elements. In regions such as inlet and outlets the structural mesh has been created with hexahedral elements to achieve exact inlet velocity profile and stabilized flow. In part of aorta arch unstructured mesh with tetrahedral element has been used.
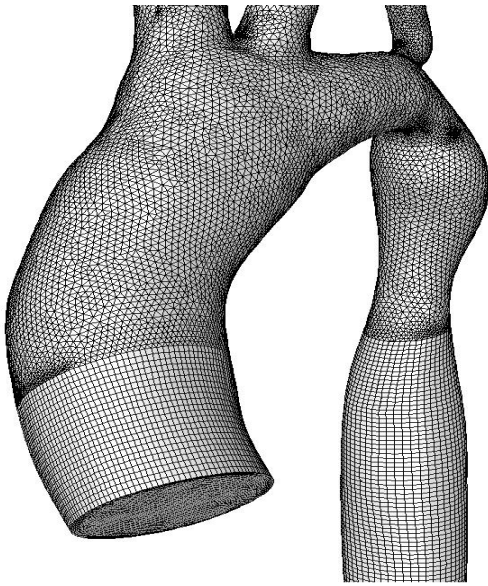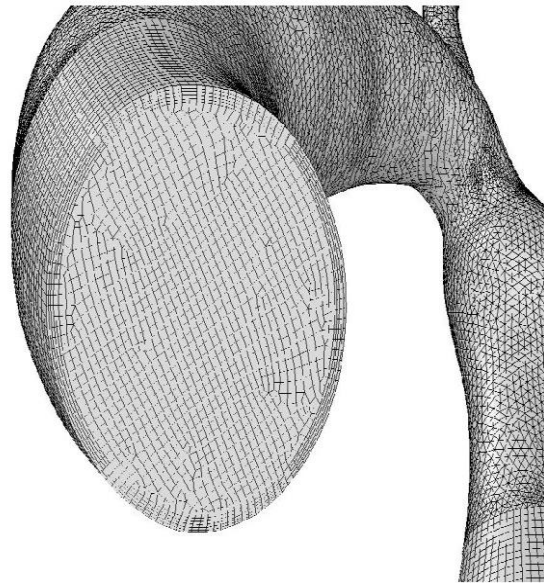
| Figure 2: Generated hybrid mesh | Figure 3: Generated mesh in the inlet of the domain |

Before the start of the numerical simulation of the blood flow the quality of mesh has been verified. Elements of mesh with poor quality has been improved. Figure 4 shows the percentage of cells with a specific orthogonal quality.
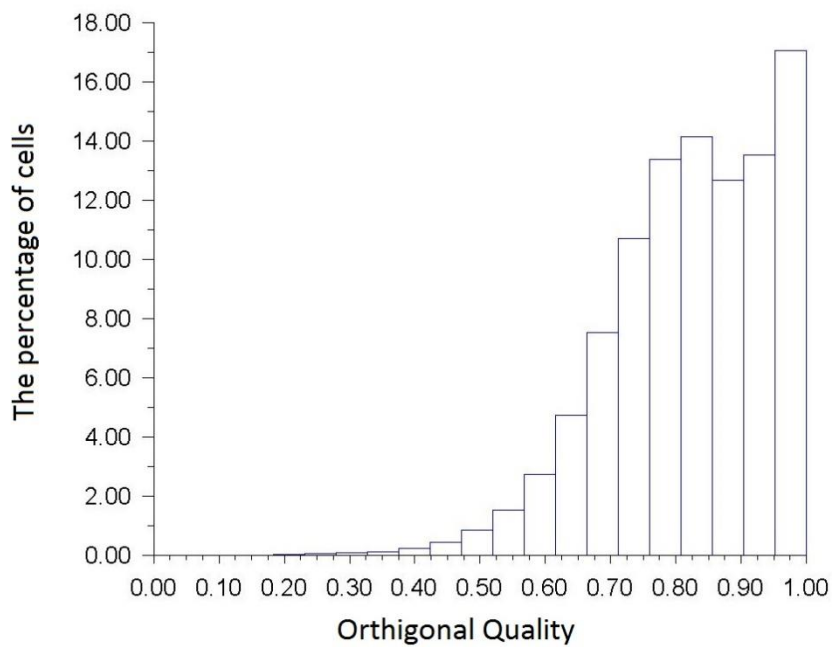

Figure 4: Histogram of the percentage of cells with a specific orthogonal quality

3. Numerical model

3.1 Model description

In presented work a comparison of numerical models of blood flow in human artery has been made. The blood was treated as a multiphase fluid that consists plasma, RBC (red blood cells) and WBC (white blood cells) and also, as alternative, the blood was treated as a single phase non-Newtonian fluid.

Multiphase model

For multiphase model the principle of mass conservation equation for fluid phase (plasma) is presented by Eq. (1) while for each solid phase (RBC and WBC) by Eq. (2). Both mass conservation equations are equal zero because mechanism of mass exchange between phases has not been used in current model, as well as no mass source are present. In the formulas presented below index f describes plasma as a fluid phase and s describes erythrocytes and leukocytes as solid phases [16]:

$$\frac{\partial(\rho_f \varepsilon_f)}{\partial t} + \nabla \cdot (\rho_f \varepsilon_f \overrightarrow{v_f}) = 0 \tag{1}$$

$$\frac{\partial(\rho_s \varepsilon_s)}{\partial t} + \nabla \cdot (\rho_s \varepsilon_s \overrightarrow{v_s}) = 0 \tag{2}$$

where:
ρ - density, ε - volume fraction of i-phase, $\vec{v}$- interphase velocity.

The sum of volume fraction for each phase is presented by Eq. (3):

$$\varepsilon_f + \varepsilon_{WBC} + \varepsilon_{RBC} = 1 \tag{3}$$

The equations for conservation of momentum is respectively written for fluid phase (4) and applied twice separately for each solid phases RBC (5) and WBC (6):

$$\frac{\partial(\rho_f \varepsilon_f \overrightarrow{v_f})}{\partial t} + \nabla \cdot (\rho_f \varepsilon_f \overrightarrow{v_f} \overrightarrow{v_f}) = \rho_f \varepsilon_f \vec{g} - \varepsilon_f \nabla P + \nabla \cdot \overrightarrow{\overrightarrow{\tau_f}} + \sum_{s=1}^{N_s}(K_{sf}(\overrightarrow{v_s} - \overrightarrow{v_f})) \tag{4}$$

$$\frac{\partial(\rho_{RBC} \varepsilon_{RBC} \vec{v}_{RBC})}{\partial t} + \nabla \cdot (\rho_{RBC} \varepsilon_{RBC} \vec{v}_{RBC} \vec{v}_{RBC})$$
$$= \rho_{RBC} \varepsilon_{RBC} \vec{g} - \varepsilon_{RBC} \nabla P - \nabla P_{RBC} + \nabla \cdot \vec{\vec{\tau}}_{RBC} + K_{f,RBC}(\overrightarrow{v_f} - \vec{v}_{RBC}) \tag{5}$$
$$+ (K_{WBC,RBC}(\vec{v}_{WBC} - \vec{v}_{RBC}))$$

$$\frac{\partial(\rho_{WBC} \varepsilon_{WBC} \vec{v}_{WBC})}{\partial t} + \nabla \cdot (\rho_{WBC} \varepsilon_{WBC} \vec{v}_{WBC} \vec{v}_{WBC})$$
$$= \rho_{WBC} \varepsilon_{WBC} \vec{g} - \varepsilon_{WBC} \nabla P - \nabla P_{WBC} + \nabla \cdot \vec{\vec{\tau}}_{WBC} + K_{f,WBC}(\overrightarrow{v_f} - \vec{v}_{WBC}) \tag{6}$$
$$+ (K_{RBC,WBC}(\vec{v}_{RBC} - \vec{v}_{WBC}))$$

where:
index q describes RBC or WBC and depends on configuration (while $q{\neq}s$), N_s - number of solid phase (N_s=2), P- pressure of fluid, Ps - granular pressure, $\vec{g}$ - gravitational acceleration, $\vec{\tau}$ - stress tensor, K - interphase exchange momentum coefficient

The momentum exchange coefficient between plasma and RBC was calculated using the Gidaspow model [4] which is a combination of two equations and is recommended for dense flows. The Gidaspow model uses Wen and Yu correlation (6) for low solid volume fraction (ε_s<0,2) and switches to Ergun's law (8) for flow in a porous medium for larger solid volume fraction [15,2].

When ε_f>0,8 the fluid-solid momentum exchange coefficient K is of the following form:

$$K = \frac{3}{4} C_D \frac{\varepsilon_s \varepsilon_f \rho_f |\overrightarrow{v_s} - \overrightarrow{v_f}|}{d_s} \varepsilon_f^{-2,65} \tag{7}$$

where:

$$C_D = \frac{24}{\varepsilon_f Re_s} \left[1 + 0,15(\varepsilon_f Re_s)^{0,687}\right] \tag{8}$$

when ε_f≤0,8:

$$K = 150 \frac{\varepsilon_s(1 - \varepsilon_f)\mu_f}{\varepsilon_f d_s^2} + 1,75 \frac{\rho_f \varepsilon_f |\overrightarrow{v_s} - \overrightarrow{v_f}|}{d_s} \tag{9}$$

The momentum exchange coefficient between plasma and WBC was calculated using Wen and Yu model (6) which is applicable for dilute flows where the total secondary phase volume fraction is significantly lower than that of the primary phase. To describe solid-solid interactions the symmetric model has been used. For this model viscosity and density are calculated from volume averaged properties [13]:

$$\rho_{pq} = \varepsilon_p \rho_p + \varepsilon_q \rho_q \tag{10}$$

$$\mu_{pq} = \varepsilon_p \mu_p + \varepsilon_q \mu_q \tag{11}$$

and the diameter is defined as:

$$d_{pq} = \frac{1}{2}\left(d_p + d_q\right) \tag{12}$$

Then the exchange coefficient is calculated from the Eq. (12):

$$K = \frac{\rho_{pq} f}{6\tau_{pq}} d_p A_i \tag{13}$$

where:

$$\tau_{pq} = \frac{\rho_{pq}\left(d_{pq}\right)^2}{18\mu_{pq}} \tag{14}$$

and

$$f = \frac{C_D Re}{18} \tag{15}$$

In turn *Re* is defined by Eq. (15) and C_D by Eq. (16):

$$Re = \frac{\rho_{pq}|\overrightarrow{v_s} - \overrightarrow{v_f}|d_{pq}}{\mu_{pq}} \tag{16}$$

$$C_D = \begin{cases} 24(1 + 0{,}15Re^{0{,}687})/Re & Re \leq 1000 \\ 0{,}44 & Re > 1000 \end{cases} \tag{17}$$

Model of turbulence used during simulation was standard k-ε and has been calculated per phase [1]. Kinetic energy and its rate of dissipation are obtained from the following transport equations [7]:

$$\frac{\partial}{\partial t}(\rho k) + \frac{\partial}{\partial x_i}(\rho k u_i) = \frac{\partial}{\partial x_j}\left[\left(\mu + \frac{\mu_t}{\sigma_k}\right)\frac{\partial k}{\partial x_j}\right] + G_k + G_b - \rho\varepsilon - Y_M + S_k \tag{18}$$

and

$$\frac{\partial}{\partial t}(\rho\varepsilon) + \frac{\partial}{\partial x_i}(\rho\varepsilon u_i) = \frac{\partial}{\partial x_j}\left[\left(\mu + \frac{\mu_t}{\sigma_\varepsilon}\right)\frac{\partial\varepsilon}{\partial x_j}\right] + C_{1\varepsilon}\frac{\varepsilon}{k}(G_k + C_{3\varepsilon}G_b) - C_{2\varepsilon}\rho\frac{\varepsilon^2}{k} + S_\varepsilon \tag{19}$$

where:
G_k represents the generation of turbulence kinetic energy due to the mean velocity gradients, G_b is the generation of turbulence kinetic energy due to buoyancy, Y_M represents the contribution of the fluctuating dilatation in compressible turbulence to the overall dissipation rate. $C_{1\varepsilon}$, $C_{2\varepsilon}$ and $C_{3\varepsilon}$ are constants.

For red blood cells Partial Differential Equation as a granular temperature model was used [16]. Granular temperature for the sth solid phase is proportional to the kinetic energy of the particles random motion and is calculated from the Eq. (19):

$$\theta_s = \frac{1}{3}u_{s,i}u_{s,i} \tag{20}$$

where:
$u_{s,i}$ represents the ith component of the fluctuating solids velocity in the Cartesian coordinate system.
While the transport equation that are derived from kinetic theory takes the form as Eq. (20):

$$\frac{3}{2}\left[\frac{\partial}{\partial t}(\rho_s\alpha_s\theta_s) + \nabla\cdot(\rho_s\alpha_s\overrightarrow{v_s}\theta_s)\right] = (-p_s\overline{\overline{I}} + \overline{\overline{\tau}}_s):\nabla\overrightarrow{v_s} + \nabla\cdot\left(k_{\theta_s}\nabla\theta_s\right) - \gamma_{\theta_s} + \varphi_{ls} \tag{21}$$

where:
$(-p_s\overline{\overline{I}} + \overline{\overline{\tau}}_s):\nabla\overrightarrow{v_s}$ = generation of energy by the solid stress tensor,
$k_{\theta_s}\nabla\theta_s$= the diffusion of energy (k_{θ_s} is the diffusion coefficient)
γ_{θ_s}= the collisional dissipation of energy [10]
φ_{ls}= the energy exchange between the lth fluid or solid phase and the sth solid phase

Single phase model

In one phase model the principle of mass conservation as well as momentum conservation have been calculated as in equations above Eq. (1) and Eq. (4) in multiphase

model for fluid phase and also model standard k-ε for turbulence model has been chosen. Blood was treated as a non-Newtonian fluid. Density of blood was calculated as a weighted average of density values used for each phase of multi-fluid model.

$$\rho_b = \varepsilon_p \rho_p + \varepsilon_{RBC} \rho_{RBC} + \varepsilon_{WBC} \rho_{WBC} \tag{22}$$

3.2 Blood as a non-Newtonian fluid

Considering blood as a non-Newtonian fluid assumes that viscosity is not constant under isobaric conditions but its value changes over time. To calculate changing value of blood viscosity the Share-Rate-Dependant Method has been used. Non-Newtonian fluid flow is modeled according to the following power law for the non-Newtonian viscosity [16]:

$$\eta = K\dot{\gamma}^{n-1} H(T) \tag{23}$$

where:
K is the consistency factor, λ is the natural time or the reciprocal of a reference shear rate, n is the power-law index, $H(T)$ is the temperature dependence, known as the Arrhenius law and is calculated from Eq. (23):

$$H(T) = exp\left[\alpha\left(\frac{1}{T-T_0} - \frac{1}{T_\alpha - T_0}\right)\right] \tag{24}$$

where:
α is the ratio of the activation energy to the thermodynamic constant, T_α is a reference temperature for which $H(T)=1$, T_0 which is the temperature shift and is set to 0 (corresponds to the lowest temperature that id thermodynamically acceptable).

3.3 Boundary conditions

Particularly significant in such a detailed numerical simulation of the blood flow is to implement appropriate boundary conditions at the inlet of the computational domain that will be able to reproduce periodical cardiac cycle. At the inlet of the aorta the velocity inlet was used. Velocity profile was calculated from the conversion of the volumetric blood flow which was measured by a phase-contrast (PC) MRI sequence with through-plane velocity encoding [17]. During the procedure the measurement of the volumetric blood flow has been made 20 times. Twenty measuring points were plotted on the graph and the linear interpolation between them has been added. Figure 5 shows an ascending aortic volumetric flow profiles for all blood phases. Two black vertical lines on the Fig. 5 are representations of characteristic points (during systole and diastole) of the cardiac cycle.
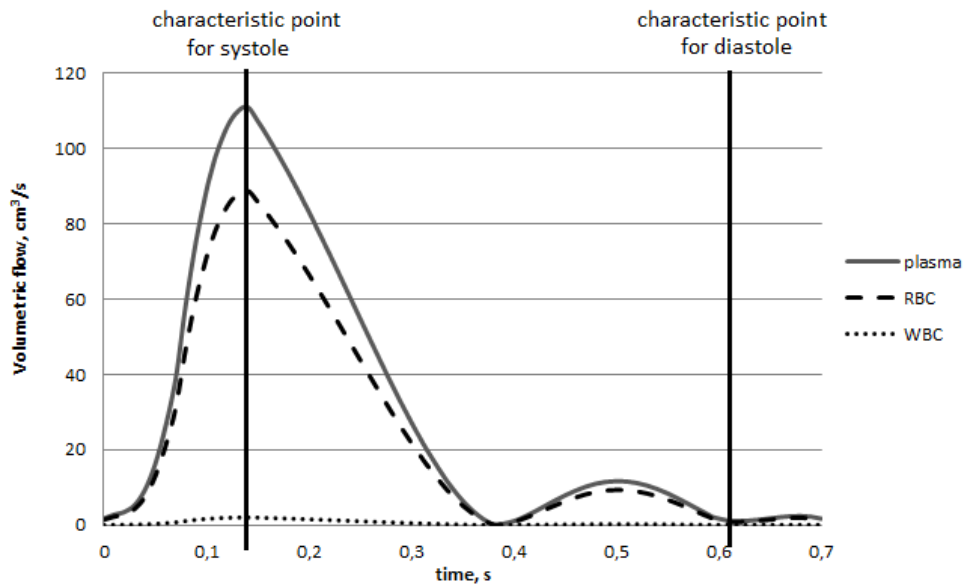
Figure 5: Volumetric blood flow at the inlet of the aorta with share of the specific phases

Pulsating and repeated boundary condition at the inlet of the computational domain was implemented by using User Defined Functions (UDFs). Profile of blood velocity is shown in Fig. 6.
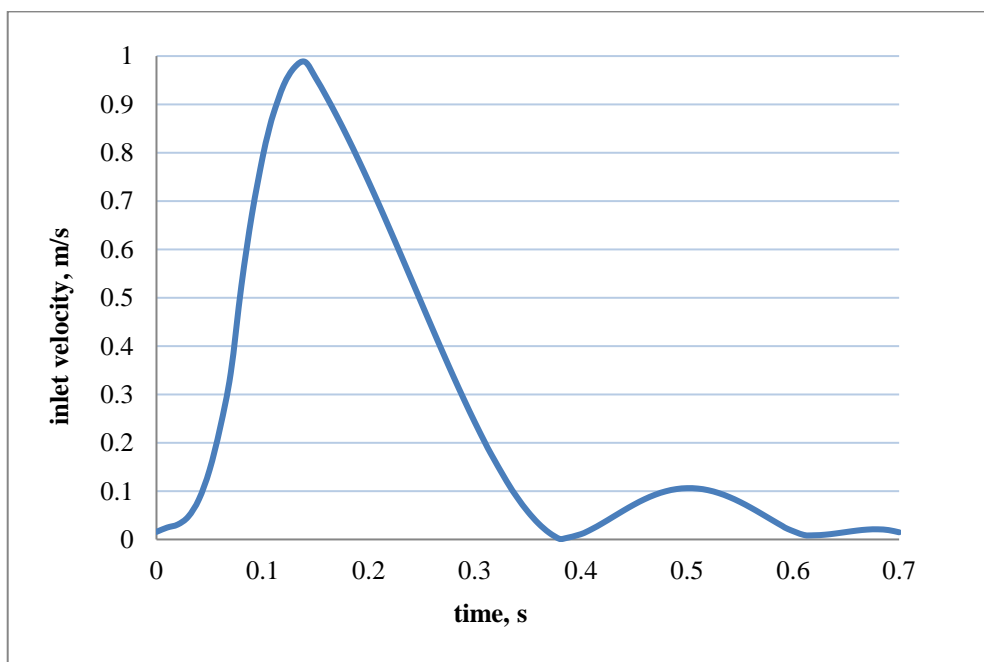

Figure 6: Velocity profile at the inlet of aorta

As the outlet boundary conditions for all branches and descending aorta the outflow condition was used. Volumetric share of blood flow through various outflows of the aortic model was measured via PC-MRI. Measurements based on [17] are presented in Table 1.

Table 1: The volumetric share of blood flow on the outlets

Location	IA	LCCA	LSA	DAO
Ascending aortic flow, %	25,6	11,3	4,3	58,8

Other important element of the blood flow simulation is to defined appropriate material properties of specific phases. The characteristic parameters (such as density [6], volume fraction and viscosity [11]) used in multiphase numerical model are shown in Table 2. It contains also coefficients describing wall behavior such as restitution coefficient that defines the amount if momentum that is retained by the particle after the collision with the boundary and specularity coefficient that is a measure of the fraction of collisions which transfer momentum to the wall [16].

Table 2: The characteristic parameters of plasma, RBC and WBC [5]

Plasma density, kg/m^3	1020
Plasma viscosity, kg/(m·s)	0,0035
RBC density, kg/m^3	1090
WBC density, kg/m^3	1050
Inlet RBC volumetric fraction, %	44
Inlet WBC volumetric fraction, %	1
Restitution coefficient	0,99999
Specularity coefficient	0,6
Time step size, s	0,01
Operating pressure, Pa	101325

Table 3 presents characteristic parameters used in single phase numerical model where blood was treated as a non-Newtonian fluid [9]. Flow rates through the upper branch vessels as well as the descending aorta are shown in Table 1.

Table 3: Characteristic parameters of blood in single phase model [9]

Blood density, kg/m^3	1051
Consistency index, kg·s^{n-2}/m	16
Power-Law index, n	0,63

4. Results

Received results present relative values of static pressure that are referred to the pressure at the inlet of the ascending aorta where the operating point was located. Possible obtained negative pressure values are relative to the adopted operating pressure outside the domain. Obtained results for single-phase and three-phase model are shown for two characteristic points of the cardiac cycle during systole (0,14s) and diastole (0,62s) as shown in Fig. 5.

Single-phase model

The pressure fields on the wall of the domain for both characteristic points for single-phase model are shown in Fig. 7. During systole the highest relative pressure occurred in the area of the inlet of the domain and it reached about 840Pa while the lowest static pressure can be noticed in the area of the coarctation of the aorta and reached about -12.4kPa. During diastole pressure at the inlet reached 4Pa and -900Pa in the stenosis of the aorta. Difference between pressure at inlet of the ascending aorta and outlet of the descending aorta was about 6kPa during systole and 80Pa during diastole.
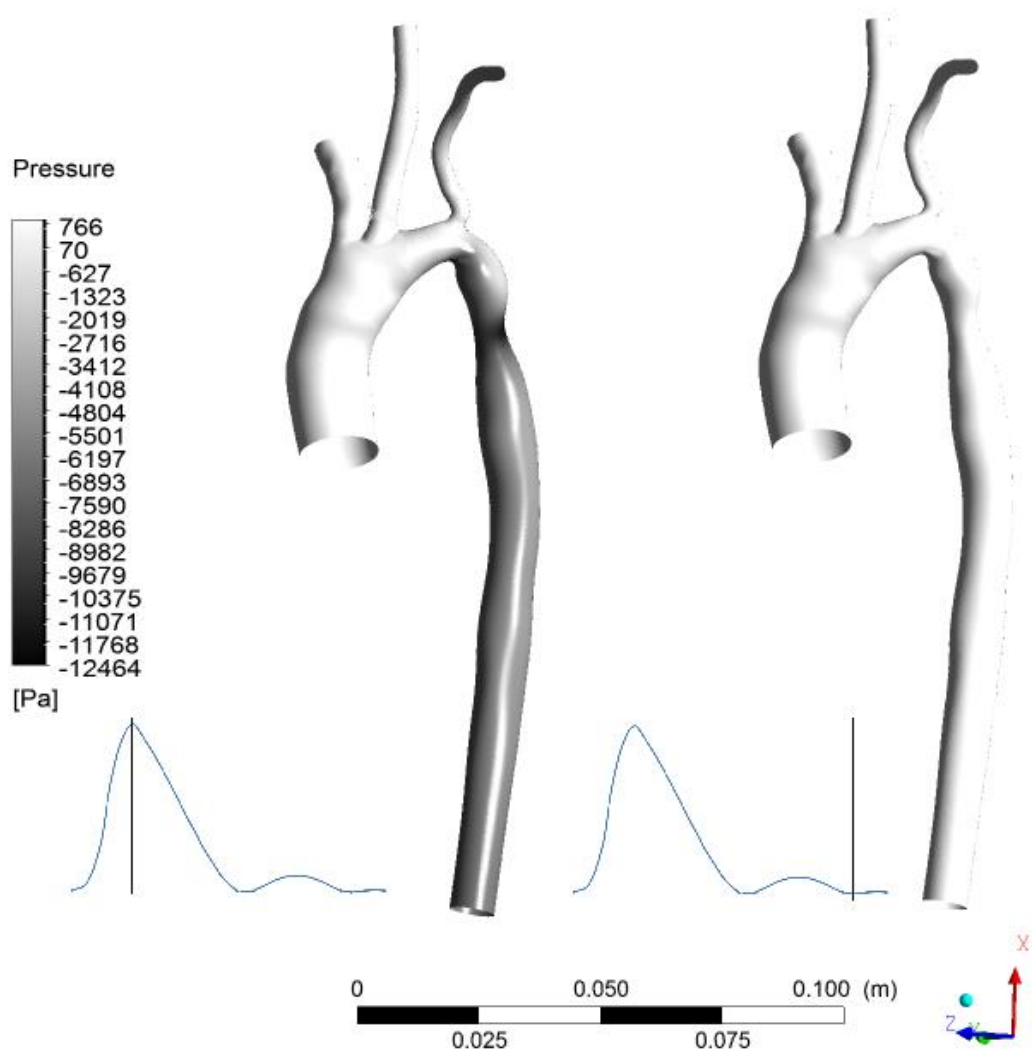
Figure 7: Comparison of pressure fields on walls during characteristic points of systole (left) and diastole (right) for single-phase model

Figure 8 shows pressure field of aortic arch with upper branches where appeared the greatest pressure changes. During systole the highest pressure values are obtained at the inlet of the domain and also at the inlet to the branches. During the diastole pressure changes are negligible.
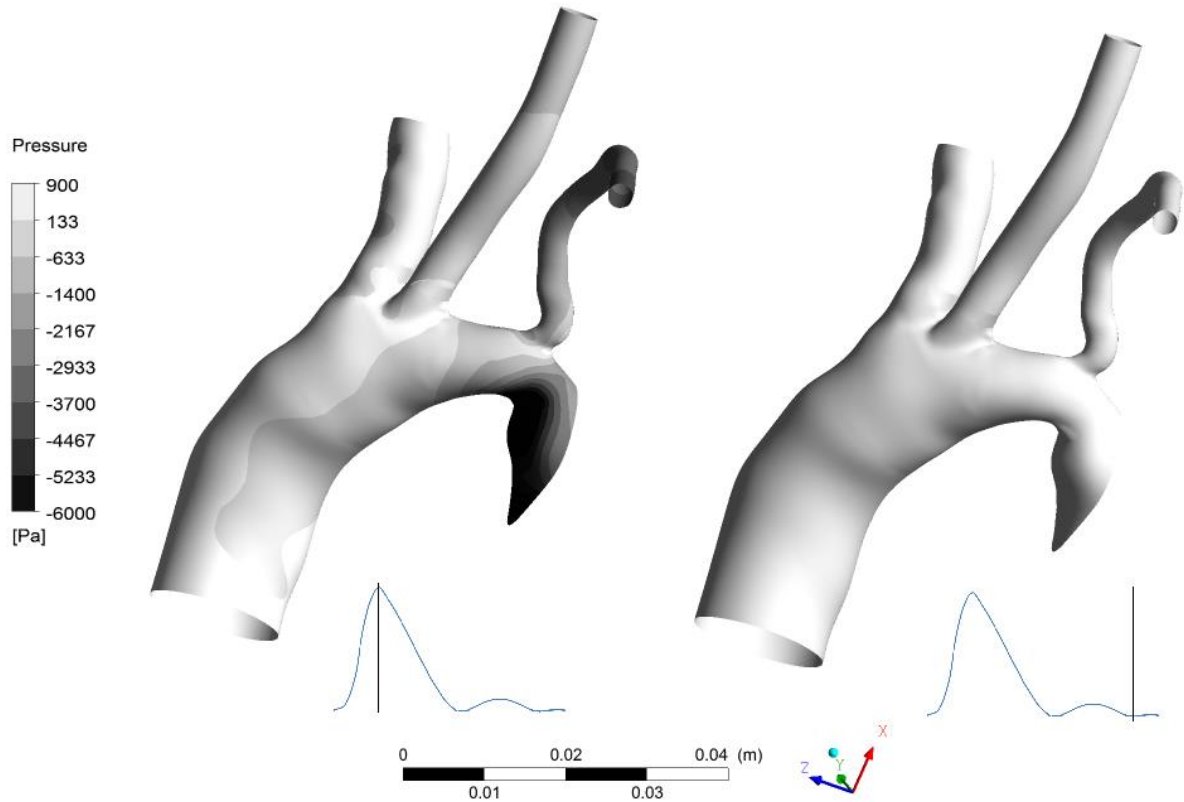

Figure 8: Comparison of pressure fields on arch of the aorta during characteristic points of systole (left) and diastole (right) for single-phase model

Wall shear stress caused by the blood flow on the rigid walls of human vessel reached the highest value of about 390Pa during systole at the bottom part of the aortic arch. High value of wall shear stress are directly related to the highest values of the velocity which are located in the same area, see Fig. 10. During diastole wall shear stress caused by blood flow was close to 2Pa on the entire surface of blood vessel. Obtained results for single-phase model are shown in Fig. 9.
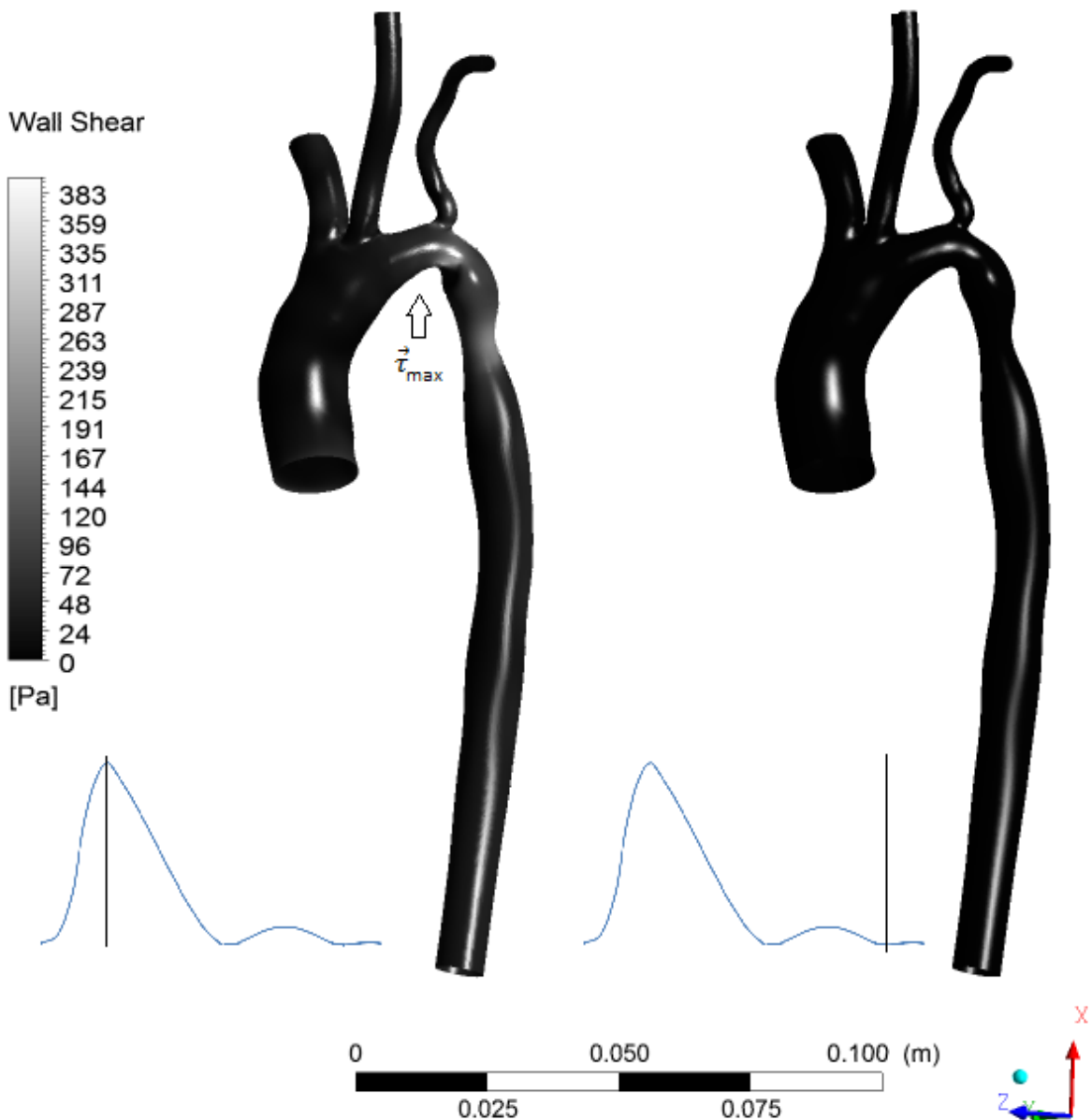
Figure 9: Comparison of wall shear stress caused by blood flow during systole (left) and diastole (right) for single-phase model

Comparison of the velocity vectors in blood vessel during systole and diastole are shown in Fig. 10. The highest velocity values appeared in the area of the aortic coarctation and on the opposite wall to the subclavian artery bifurcation on the arch of the aorta. The maximum velocity values reached almost 5m/s. During systole blood flow was mostly laminar the only eddies were located at the end of the aortic arch and near the pathological narrowing. The carried out analysis of the velocity field showed that blood flowed to the specific outflows according to the implemented boundary conditions.

During diastole velocity of blood and its volumetric flow were close to zero throughout the vessel. Blood flow was turbulent and highly irregular it is caused by the low pressure gradient between inlet and outlets of the domain, a lot of eddies are clearly visible. The reversed flow appeared in every outflow. The highest velocity values during diastole reached 0.13m/s in the region before coarctation.
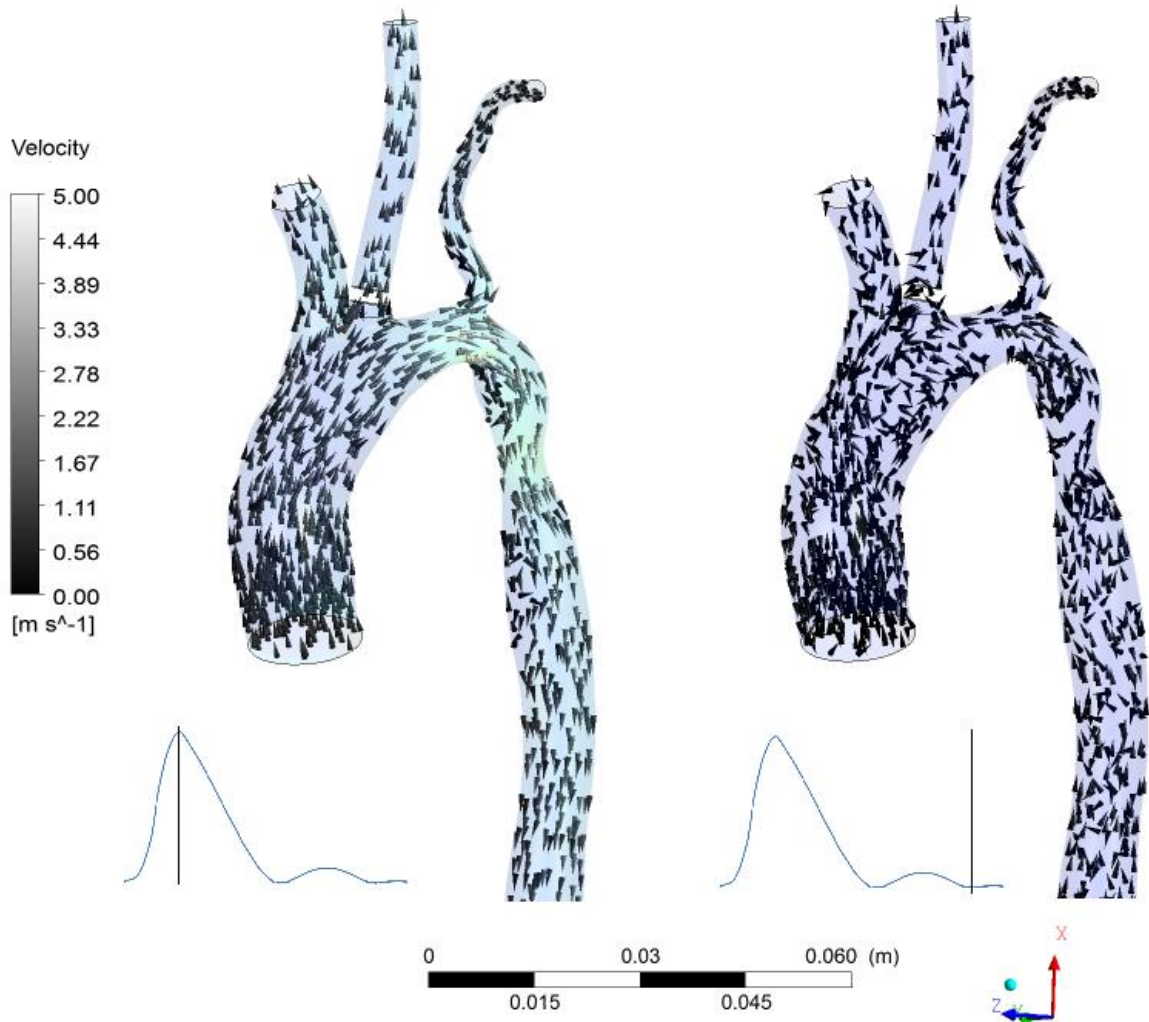

Figure 10: Comparison of velocity vectors in characteristic points during systole (left) and diastole (right) for single-phase model

Multi-phase model

Analysis of the multi-phase model shows that comparing to the single-phase model difference between pressure at the inlet to the ascending aorta and outlet of the descending aorta for mixture is lower and reaches about 4.9kPa (systole) and 30Pa during diastole. The highest static pressure of about 260Pa appeared at the inlet of the aorta and the -13.4kPa in the region of the aortic coarctation. According to the pressure profile for the characteristic point

of diastole the maximum pressure occurred at the outlet of the geometry and reached 26Pa while pressure at the inlet was about -4Pa. Pressure fields during systole and diastole are presented in Fig. 11.
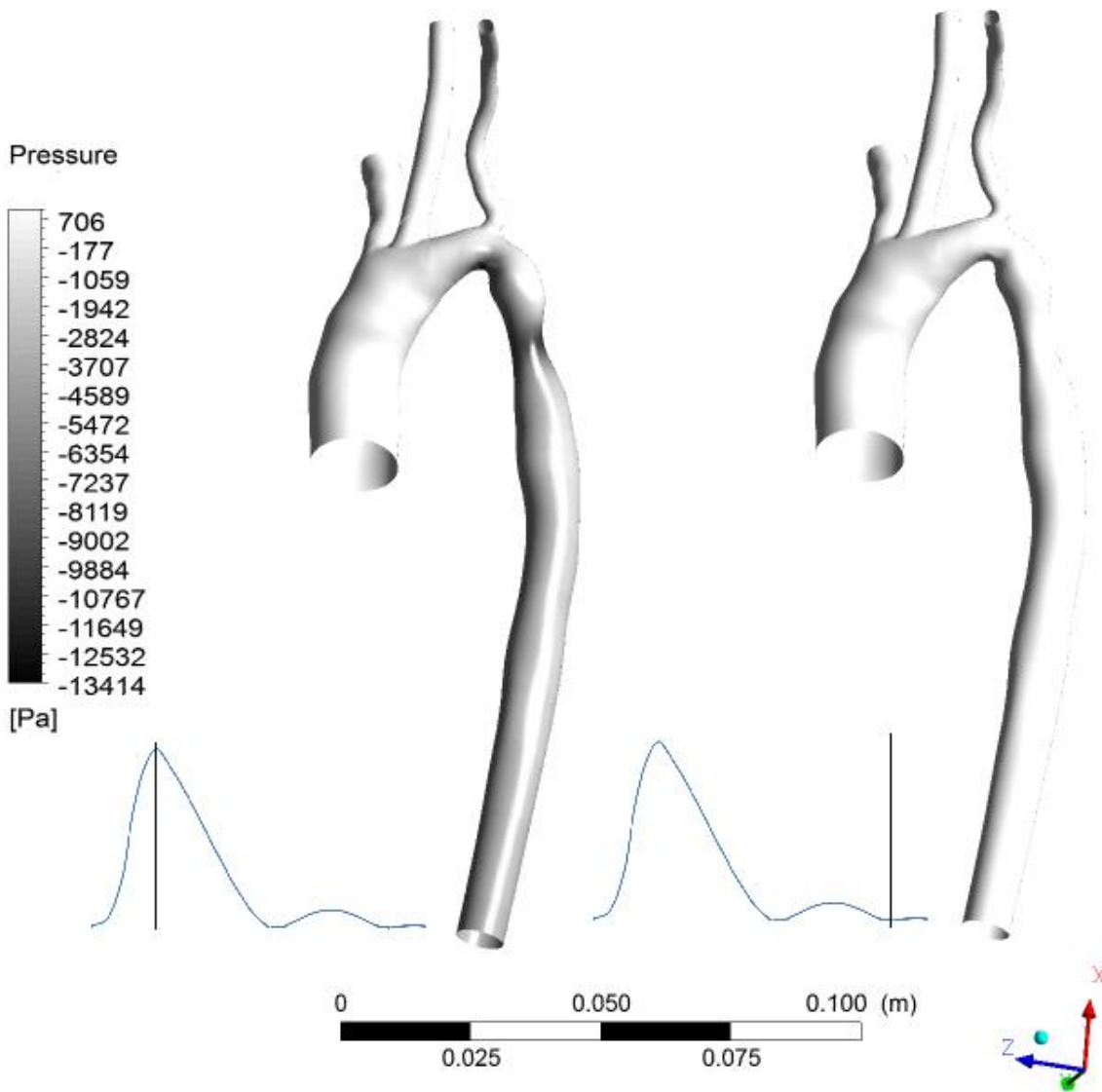

Figure 11: Comparison of pressure fields on walls during characteristic points of systole (left) and diastole (right) for multi-phase model

In multi-phase model likewise in single-phase model the largest pressure changes occur at the arch of the aorta and at the inlets to branches during the systole. While during the diastole values of the pressure changed by only few kilopascals. Obtained results are shown in Fig. 12.
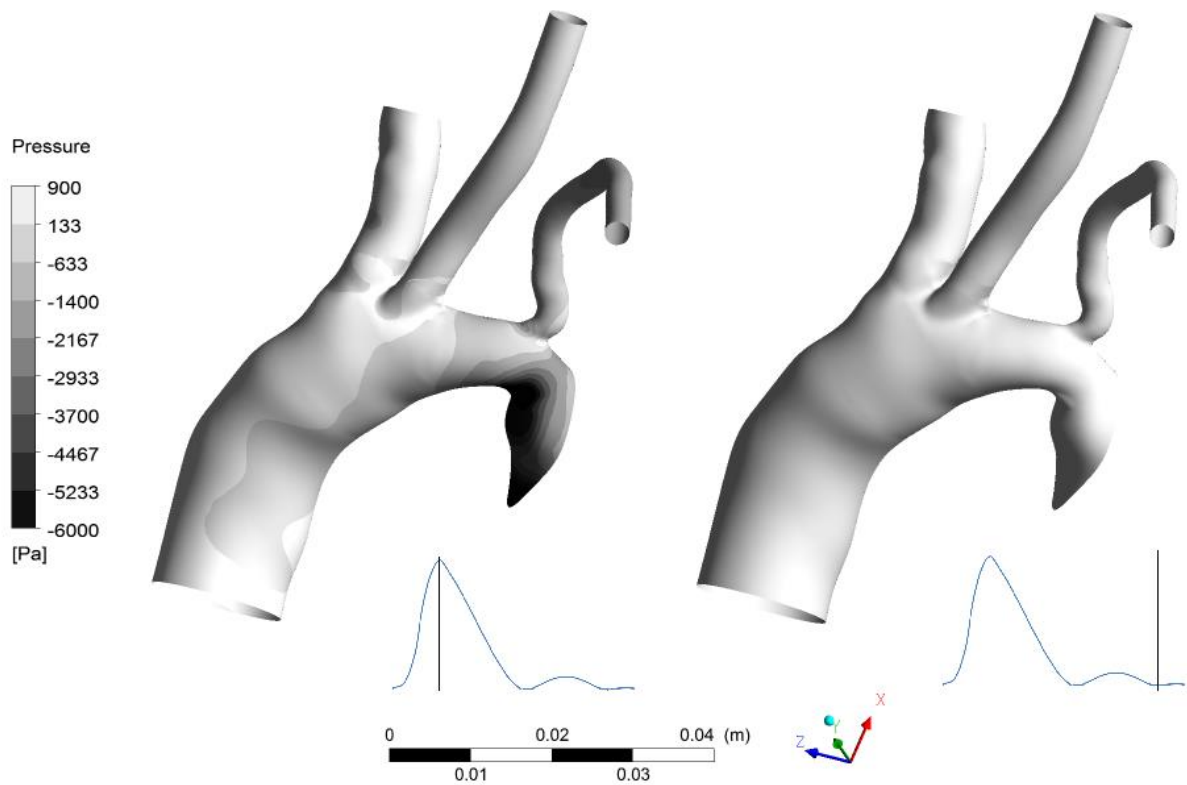
44

Figure 12: Comparison of pressure fields on arch of the aorta during characteristic points of systole (left) and diastole (right) for single-phase model

Results of the wall shear stress caused by the plasma phase flow on rigid walls of the artery show that as well as for single-phase analysis the highest value of about 95Pa appeared underneath the aortic arch on the opposite wall to the left subclivian artery. Obtained results showed in Fig. 13 are significantly lower than achieved in one-phase model. During diastole wall shear stress on entire surface of the rigid vessel was close to 2kPa. As in single-phase model areas where appeared the highest values of wall shear stress are related with locations where are obtained the highest values of velocity.
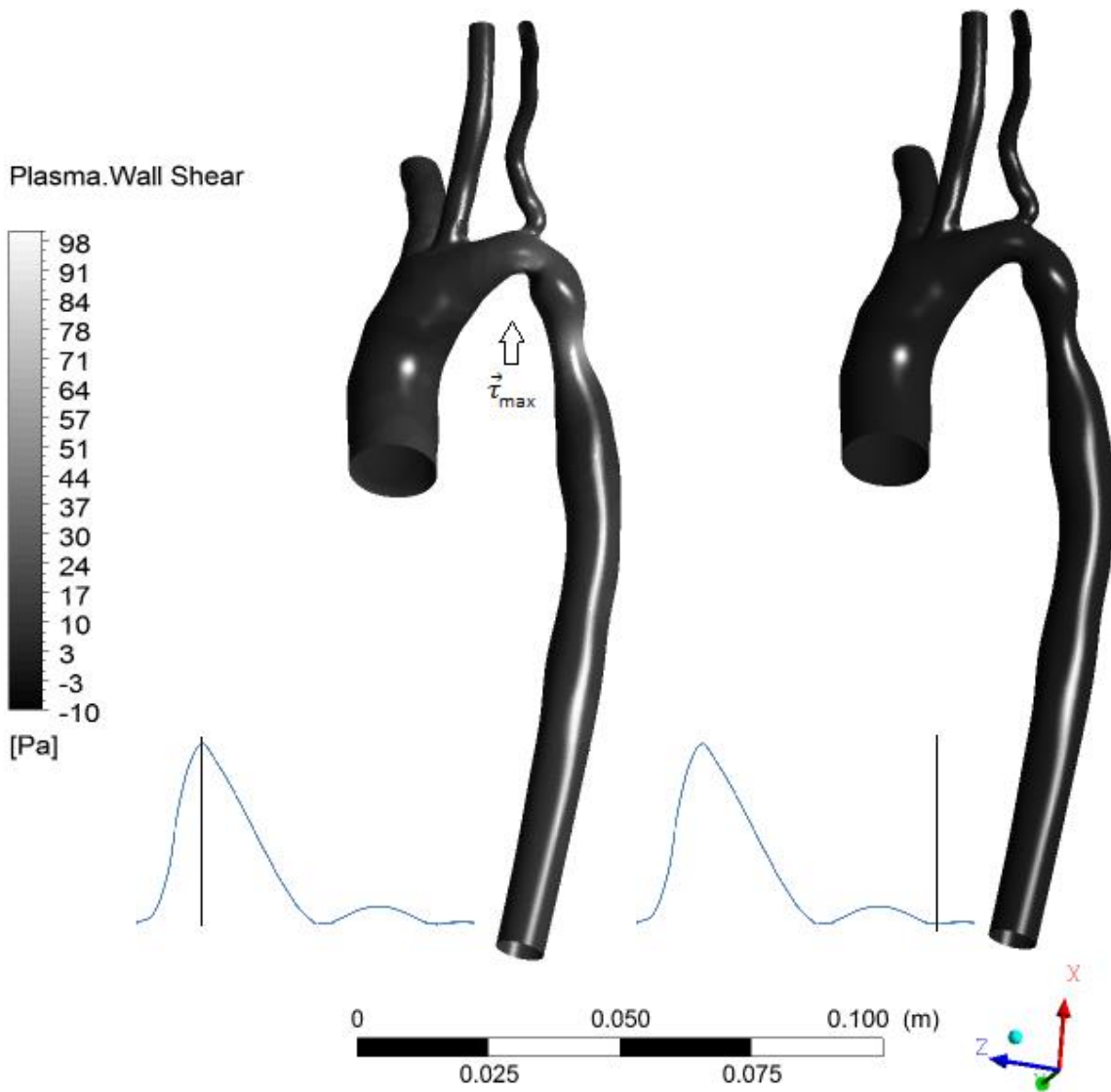
Figure 13: Comparison of wall shear stress caused by blood flow during systole (left) and diastole (right) for multi-phase model

Wall shear stress caused by erythrocytes during systole is shown in Fig. 14. Calculated values are almost three times bigger than for plasma flow and the highest value reaches about 230Pa in the region of arch of the aorta. Wall shear stress caused by leukocytes during systole is negligible and the highest value does not exceed 1Pa, results are shown in Fig. 15.
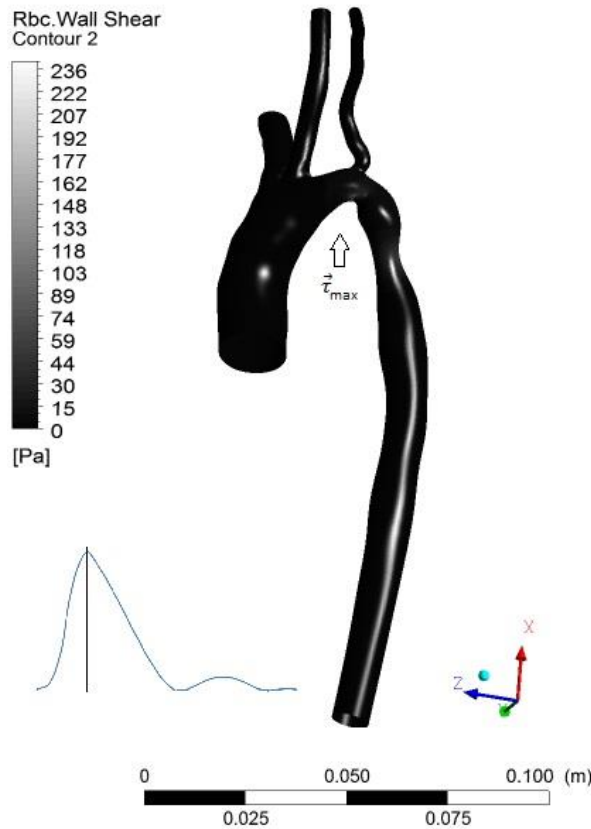
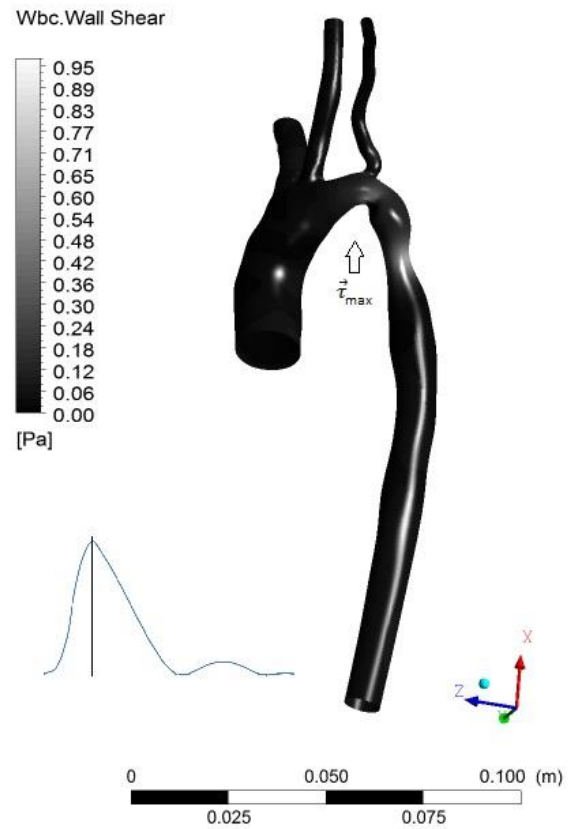Figure 14: Wall shear stress during systole for RBC phase

Figure 15: Wall shear stress during systole for WBC phase

The velocity vectors obtained at characteristic points of systole and diastole has been compared in Fig. 16. The simulated flow and calculated velocity profiles for plasma flow in three-phase model looks similar to blood flow in one-phase model. The highest velocity values are present at the area of coarctation and aortic arch and during systole reached over 4m/s. The lowest values appears to be located close to the wall surface. According to the velocity field analysis, during systole blood flow was stable and mostly laminar, while during diastole flow was highly irregular and turbulent, also in every outlet occurred the reversed flow.
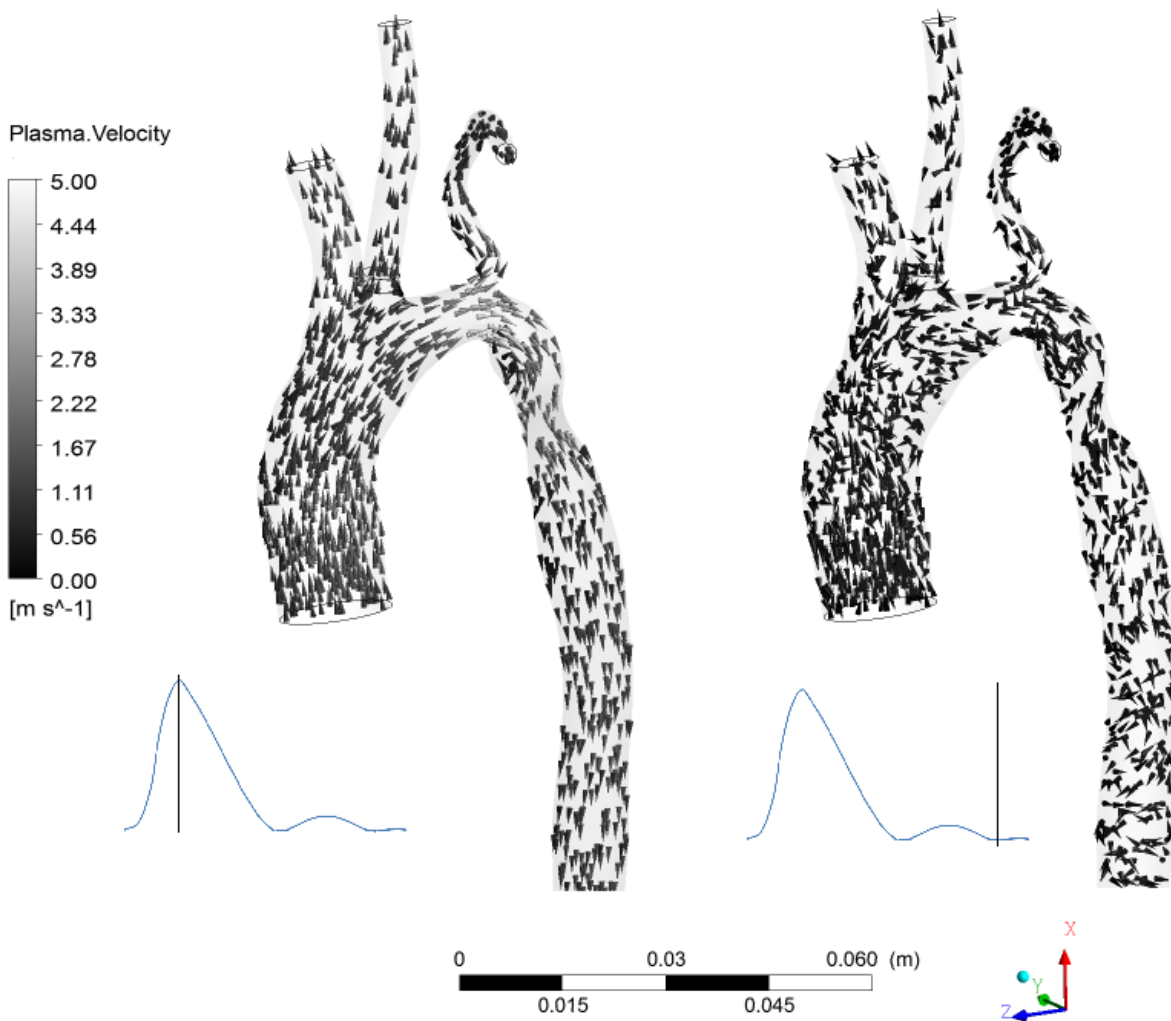
Figure 16: Comparison of velocity vectors in characteristic points during systole (left) and diastole (right) for multi-phase model

5. Conclusions

The main scope of the present work was to show an Euler-Euler multiphase approach in model of blood flow in human blood vessel (artery) section. In paper blood flow within real geometry of a 8-year old female patient diagnosed with moderate thoracic aortic coarctation has been simulated. Numerical analysis consists of multi-phase model where blood was a non-homogenous mixture of three phases. As primary phase plasma as a Newtonian fluid was used and as a secondary phases two granular phases RBC and WBC which represents morphotic elements of blood. In multi-fluid model each phase was treated as a separate continuum and modeled using Eulerian approach. Second numerical analysis consists single-

phase model where blood was treated as a homogenous, non-Newtonian mixture with average properties. To reproduce periodical cardiac cycle the velocity profile as boundary condition on the inlet of the domain has been implemented using User Defined Functions. Boundary conditions applied in project are simplification of the influence that circulatory system exerts on modeling section of the aorta. To fully compensate the influence of the human circulatory system the numerical model should be coupled with an electrical analog (lumped model). Presented model assumed rigid walls of the blood vessel and thus that the wall motion affects the flow insignificantly. This simplification could have impact on the obtained pressure and velocity profiles. Presented results show pressure field, wall shear stress and velocity vectors for two characteristic points of cardiac cycle (during systole and diastole) for both single-phase and multi-phase models.

Acknowledgments

Refrences

[1] Anderson J., *Computational fluid dynamics. The basics with applications* McGraw-Hill, New York (1995)

[2] Ergun S. Fluid Flow through Packed Columns, *Chemical Engineering Progress* (1952) **48**(2):89–94

[3] Gidaspow. D., *Flow and Fluidization, Academic Press*, Boston, MA., Reaction Engineering International (1994)

[4] Gidaspow D., Bezburuah R. and Ding J., *Hydrodynamics of Circulating Fluidized Beds, Kinetic Theory Approach*, In: Fluidization VII, Proceedings of the 7th Engineering Foundation Conference on Fluidization, 75–82 (1992).

[5] Huang J., Lyczkowski R. W., Gidaspow D., Pulsatile flow in a coronary artery using multiphase kinetic theory, *Journal of Biomechanics* (2009) **42**: 743-754

[6] Kenner T., The measurement of blood density and its meaning, *Basic Research in Cardiology* (1989) **84**:111-124

[7] Launder B. E. and Spalding D. B., *Lectures in Mathematical Models of Turbulence*. Academic Press, London, England (1972)

[8] Laurent F., Massot M., Villedieu P., Eulerian multi-fluid modeling for the numerical simulation of coalescence in polydisperse dense liquid sprays, *Journal of Computational Physics*, (2004) **197:**505-543.

[9] Liu B., Tang D., Influence of non-Newtonian Properties of Blood on the Wall Shear Stress in Human Atherosclerotic Right Coronary Arteries, *Mol Cell Biomech* (2011) **8**(1):73-90, doi: 10.3970/mcb, 2011

[10] Lun C. K. K., Savage S. B., Jeffrey D. J., Chepurniy N., Kinetic Theories for Granular Flow: In elastic Particles in Couette Flow and Slightly Inelastic Particles in a General Flow Field, *J. Fluid Mech.*(1984) **140**:223–256

[11] Siebert M. W., Fodor P. S., *Newtonian and Non-Newtonian Blood Flow over a Backward-Facing Step - A Case Study*, COMSOL Conference, Boston (2009)

[12] Stergiopulos N., Computer simulation of arterial blood flow. *Retrospective Theses and Dissertations*. Paper 9896, 1990

[13] Syamlal M *The Particle-Particle Drag Term in a Multiparticle Model of Fluidization* National Technical Information Service, Springfield (1987)

[14] Tu J., Yeoh G.H., Liu Ch., *Computational Fluid Dynamics, A Practical Approach*, Elsevier (2008)

[15] Wen C.-Y. and Yu Y. H., Mechanics of Fluidization, *Chemical Engineering Progress Symposium Series* **62**:100-111(1966)

[16] ANSYS Academic Research, Release 17.0, *Help System, UDF Manual*, ANSYS, Inc.

[17] CFD Challenge problem: http://www.vascularmodel.org/miccai2012 (accessed May 16th 2016)

Wielofazowy model przepływu krwi w naczyniu krwionośnym ze sztywnymi ścianami w podejściu Euler-Euler

Maria Gracka

Słowa kluczowe: CFD, model Euler-Euler, przepływ wielofazowy, aorta, przepływ krwi

Streszczenie

Choroby oraz zaburzenia układu krążenia, takie jak miażdżyca tętnic, udary i zawały serca są główną przyczyną zgonów na świecie, w szczególności w rozwiniętych i uprzemysłowionych społeczeństwach. Zrozumienie podstawowych mechanizmów i zjawisk występujących w układzie sercowo-naczyniowym może być przydatne do wczesnego wykrycia i diagnozy rozwijających się zmian w naczyniach krwionośnych. W prezentowanej pracy przeprowadzono analizę numeryczną przepływu krwi w aorcie. Wykonano dwa modele numeryczne pierwszy model traktujący krew jako jednorodną ciecz nienewtonowską z reologicznymi właściwościami średnimi dla lepkości i gęstości składników.   Drugi model obejmuje analizę przepływu krwi będącej mieszaniną trzech faz (osocza, czerwonych krwinek oraz białych krwinek). Symulacje przeprowadzono przy użyciu komercyjnego oprogramowania ANSYS Fluent (ANSYS Inc., USA). W projekcie wykorzystano geometrię aorty 8-letniej pacjentki z koarktacją za łukiem aorty (zwężenie ok. 65%) wygenerowaną ze skanu wykonanego podczas wzmocnionej angiografii (MRA). Model obejmuje aortę wstępującą, łuk aorty, aortę zstępującą oraz górne odgałęzienia naczyń (pień ramienno-głowowy, tętnicę szyjną wspólną oraz podobojczykową lewą). W celu odwzorowania cyklu

pracy serca na wlocie do aorty jako warunek brzegowy przyjęto profil prędkości przeliczony z przepływu objętościowego krwi, który zmierzono w trakcie badania kontrastem fazowym. Warunek zaimplementowano wykorzystując tzw. procedury własne (UDF - User Defined Function). Jako warunek brzegowy na wylotach przyjęto wypływy przez odgałęzienia oraz aortę zstępującą, których wartość wyrażona jest udziałem procentowym ze strumienia krwi na wlocie do aorty wstępującej. Wyniki symulacji numerycznej przedstawiono dla dwóch punktów charakterystycznych podczas skurczu i rozkurczu serca.